JOURNAL OF FORENSIC SCIENCES

J Forensic Sci, March 2010, Vol. 55, No. 2
doi: 10.1111/j.1556-4029.2009.01272.x
Available online at: interscience.wiley.com

PAPER

CRIMINALISTICS

Jennifer R. Verkouteren,[1] *M.S.; Jessica L. Coleman,*[1] *M.S.; and Inho Cho,*[2] *B.S.*

Automated Mapping of Explosives Particles in Composition C-4 Fingerprints*†‡

ABSTRACT: A method is described to perform automated mapping of hexahydro-1,3,5-trinitro-1,3,5-triazine (RDX) particles in C-4 fingerprints. The method employs polarized light microscopy and image analysis to map the entire fingerprint and the distribution of RDX particles. This method can be used to evaluate a large number of fingerprints to aid in the development of threat libraries that can be used to determine performance requirements of explosive trace detectors. A series of 50 C-4 fingerprints were characterized, and results show that the number of particles varies significantly from print to print, and within a print. The particle size distributions can be used to estimate the mass of RDX in the fingerprint. These estimates were found to be within ±26% relative of the results obtained from dissolution gas chromatography/μ-electron capture detection for four of six prints, which is quite encouraging for a particle counting approach. By evaluating the average mass and frequency of particles with respect to size for this series of fingerprints, we conclude that particles 10–20 μm in diameter could be targeted to improve detection of traces of C-4 explosives.

KEYWORDS: forensic science, trace detection, polarized light microscopy, explosives, particle counting, fingerprints, automated imaging

The detection of trace amounts of explosives at airports and other security venues is an important component of counterterrorism efforts. Currently, over 10,000 ion mobility spectrometry (IMS)-based explosive trace detectors (ETDs) are deployed at airports worldwide (1), in addition to the number used by the U.S. military and other federal agencies. The two general forms of ETDs are desktop instruments that use physical swiping for sample collection, and personnel screening portals that remove particles with controlled air jets. A critical aspect of the deployment of ETDs is the calibration and testing of those instruments at the relevant threat levels. Fingerprints are considered to be one of the primary mechanisms for the transfer of trace amounts of explosives during bomb handling and preparation, and one of the targeted types of samples for collection (2). Critical properties that must be understood about these samples include the total mass and particle sizes of the explosives. The detection limits of ETDs are based on mass, but the collection efficiency of the sample is dependent on particle size.

The amount of explosives found in fingerprints will necessarily depend on the amount of contamination originally present on the hands, and the number of successive impressions made after contamination. An early study evaluated the mass of hexahydro-1,3,5-trinitro-1,3,5-triazine (RDX) in C-4 fingerprints prepared under controlled conditions (3). Composition C-4 military explosive typically contains 91% RDX, 5% dioctyl sebacate or adipate, 2% polyisobutylene, and 2% oil (4). In the Gresham et al. (3) study, the prints were prepared in series from the first impression to the 50th impression following a single contamination event. The goal was to demonstrate a predictable change in the mass of RDX with respect to fingerprint number in the series. In this manner, a method would be available to produce fingerprints containing approximately known amounts of explosive that could be used for testing ETDs. The mass of RDX was found to decrease from micrograms in the first print to nanograms in the 50th, but with a higher variability from print to print than expected. This variability reduced the utility of such a method to produce useful test materials. Variability in fingerprints produced from explosives was also noted by Phares et al. (5), and they speculated that this might be due to differences in applied force or humidity.

A more recent study conducted by one of the authors of this paper evaluated the particle size distribution of RDX particles in C-4 fingerprints (6). The study demonstrated that RDX particles in fingerprints have particle size distributions indicative of fragmentation of RDX crystals, and that the particles ranged in diameter from less than 1–100 μm or larger. The mass of RDX in the fingerprints as a whole was found to be concentrated in the larger particles. A small change in the number of large particles could be a source of the variability seen by Gresham et al. (3). To evaluate the variability in the numbers of RDX particles present in fingerprints, we needed to characterize a large number of samples, which necessitated improvements in the polarized light microscopy (PLM) method used in our first study. Our earlier work employed manual counting of particles in an oil immersion preparation, which is

[1]National Institute of Standards and Technology, Gaithersburg, MD.
[2]Transportation Security Laboratory, Atlantic City International Airport, NJ.

*The Department of Homeland Security Science and Technology Directorate sponsored this work under an Interagency Agreement with the National Institute of Standards and Technology.
†Presented at the 9th International Symposium on the Analysis and Detection of Explosives in Paris, France, July 2–6, 2007.
‡Certain commercial equipment, instruments, or materials are identified in this document. Such identification does not imply recommendation or endorsement by the National Institute of Standards and Technology, nor does it imply that the products identified are necessarily the best available for the purpose.

Received 15 Dec. 2008; and in revised form 13 Jan. 2009; accepted 31 Jan. 2009.

impractical for the evaluation of a large number of prints. Immersion of the sample in oil also created a number of difficulties, specifically with postextraction of the explosive for dissolution analysis.

In this work, we describe an automated PLM procedure for counting and sizing explosives particles in fingerprints made from C-4. We use both plane polarized light and crossed polarized light to produce complete images of the fingerprints, and also the size, shape, and locations of the RDX particles. A series of 50 prints was made from C-4, from which 36 were characterized to determine particle size distributions of the RDX particles. For selected fingerprints, the mass of RDX was determined by two techniques, calculation based on the particle size and number, and direct dissolution analysis using gas chromatography/μ-electron capture detection (GC/μ-ECD). The automated PLM method can be used to rapidly characterize C-4 fingerprints with relatively little operator input, so that a large number of samples can be evaluated. This will aid in the development of "threat libraries" that contain particle size and number information for a number of samples, and therefore delineate the performance requirements for ETDs. In addition, the PLM analysis is nondestructive and the samples can be used after characterization as test materials for ETDs.

Methods

Preparation of C-4 Fingerprints

Glass microscope slides were used as the substrate for the fingerprints prepared in this study. The slides were cleaned prior to use to ensure a low background in crossed-polarized light. The cleaning process started with a soap solution, using gloved fingers to rub the slides, which were then rinsed with filtered, distilled water. The slides were then placed in a beaker containing ethanol and sonicated for 15 min. The final step was to dry the slides using filtered air.

A sample of C-4 was selected from the repository maintained at the Transportation Security Laboratory (Atlantic City International Airport, NJ). The fingerprints were prepared in a laboratory maintained at temperatures between 25.5°C and 26.5°C and relative humidities of 50–60%. To prepare the C-4 sample to make fingerprints, a 100 ± 5 mg slice of C-4 was placed on a glass slide. A second glass slide was placed on top, and the slides were squeezed together to create a thin layer of C-4. The slides were then separated, resulting in a split sample with deposits on both slides. The thumb was contaminated by placing it on one of the split samples for 3 min, allowing the thumb and explosive surface to equilibrate. The thumb was then lifted, and the glass slide was allowed to fall off by the force of gravity. A print was applied to each precleaned glass slide by placing the slide on a scale and applying the thumb with *c.* 6.8 kg of force. A series of prints (1–50) were collected, labeled, and stored in clean, plastic microscope slide containers.

Particle Imaging

An Olympus (Center Valley, PA) BH-2 PLM was used to collect images of the RDX particles in the C-4 prints. (Certain commercial equipment, instruments, or materials are identified in this document. Such identification does not imply recommendation or endorsement by the National Institute of Standards and Technology [NIST], nor does it imply that the products identified are necessarily the best available for the purpose.) Automated stage movement and image collection were used to produce complete maps of each print and to minimize operator input and time of analysis. The system includes a Prior ProScan X-Y-Z sample stage (Prior Scientific Inc., Rockland, MA) with a repeatability of ±1 μm and an Evolution MP digital CCD cooled color camera (Media Cybernetics Inc., Silver Spring, MD). Control over the automation, including stage movement and image collection, was accomplished through the software program ImagePro (Media Cybernetics Inc.). Magnification calibration was accomplished through use of a calibration slide provided by Media Cybernetics, and then tested using a microscopy size standard produced by Geller Microanalytical Laboratory (Topsfield, MA) and traceable to NIST. Thirty-six fingerprints were selected arbitrarily from the series of 50 to analyze. The fingerprints were imaged in their entirety by collecting "tiled" images. For a tiled image, the area is subdivided into smaller, consecutive "tiles" that are individual images collected at a higher magnification. The tiles are stitched together to form one large image that has a total pixel count that is the sum of all the tiles. For the fingerprints, each tile was collected with a 5× objective at a camera resolution of 640 × 480 pixels to yield 2.7 μm/pixel. The thumbprints evaluated in this study are *c.* 29 × 18 mm, requiring over 200 tiles to fill (Fig. 1).

Two tiled images were collected for each print: the image of the visible print and the image of the RDX particles. The fingerprint image was collected with transmitted plane polarized light and the RDX particle image was collected with transmitted crossed polarized light. RDX particles are the major birefringent phase in C-4 fingerprints, and can be imaged on this basis using crossed polarized light (6). The only other birefringent materials typically found in C-4 prints are organic fibers, which generally can be distinguished on the basis of shape. The fingerprints were analyzed dry without any sample preparation. Although superior imaging conditions can be achieved with oil immersion and a coverslip, we accepted the slightly poorer imaging obtained from dry samples because of the difficulties presented by oil immersion. Oil immersion removes most of the contrast observed for the visible print, precludes the use of many alternative approaches for mass determination, results in particle movement, and interferes with the measurement of particle thickness.

To start the imaging process, fiducial marks were drawn at two corners of the fingerprint to describe a bounding rectangle (one of the fiducial marks is visible in Fig. 1). This was performed by eye by tilting the glass slide to obtain the best contrast to observe the print. All prints in the series of 50 were visible using this approach, although the last few prints were very faint and the boundaries were not as easy to discern. The fiducial marks were placed conservatively to just enclose the fingerprint and minimize the size of the tiled images. The average size of the tiled images is *c.* 100,000 kb, which is large but can be accommodated by the computer used to collect and process the images. In the future, we will probably use a smaller finger to reduce the total size of the prints.

For each imaging mode (visible print image or RDX image), optimal configurations of microscope and camera parameters were determined and used for all prints. For the fingerprint image, the intensity of the microscope lamp was set near the minimum position, and the substage condenser aperture was closed by *c.* 75%. To produce a seamless image of the print, a background correction procedure was used. An image of the background was collected at a position outside the borders of the print and used to correct each tile with a background subtraction procedure available in the ImagePro software package. For the crossed polarized light image, the intensity of the microscope lamp was placed near the maximum value, and the substage condenser aperture was opened almost completely. Because the background is almost completely black, no background correction procedure was required for the crossed polarized light image.

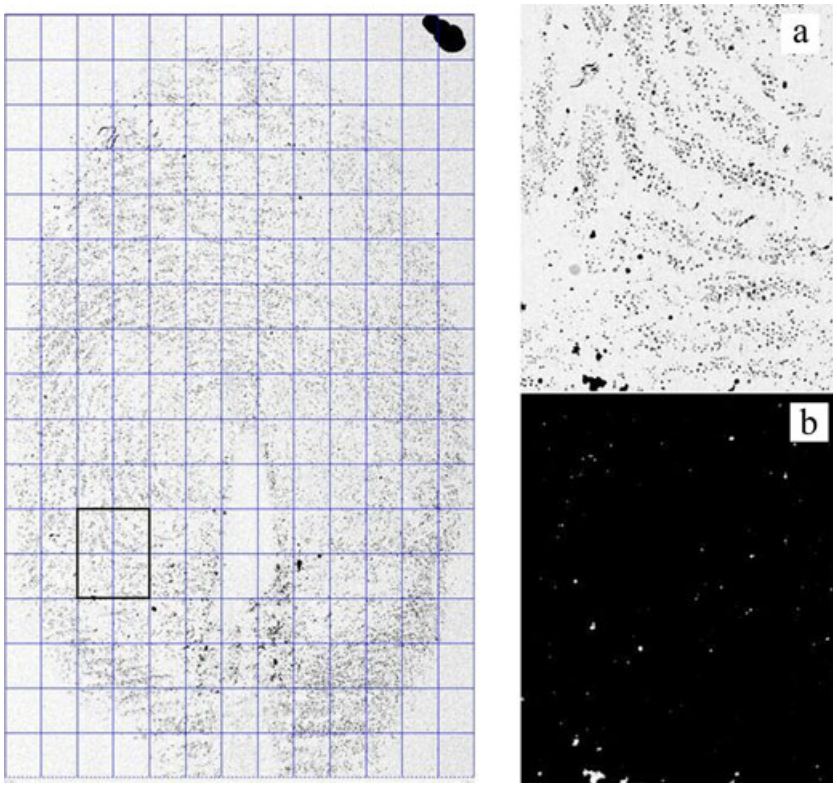

FIG. 1—*Plane polarized light image of visible fingerprint on left with overlay of grid pattern showing sizes of individual tiles used to collect the image. Selected area marked by bold box is shown in plane polarized light in (a) and crossed polarized light in (b). RDX particles are the birefringent (bright) particles observed in the crossed polarized light image.*

To image a single print, the slide is placed in the mechanical stage and held firmly by the spring arm mechanism. The positions of the fiducial marks are registered, and the number of tiles required to completely fill the bounding rectangle is calculated by the program. The microscope and camera are configured for visible print imaging and the tiled image is collected. The slide is left in place, and the microscope and camera reconfigured for crossed polarized light to collect the image of the RDX particles. A tiled image takes *c.* 15 min to collect, including setting up the imaging conditions and registering the fiducial marks. The slide is not moved between collections of the two tiled images to allow for complete registration of the images. When the images are registered with respect to each other, comparisons can be made easily between the two images to evaluate the locations of the RDX particles with respect to the visible print (Fig. 1*a* and *b*).

The smallest particle that can be counted in the tiled images is 2.7 μm in diameter (equivalent to 1 pixel). To provide improved counting of the smaller particles, and to image particles smaller than 1 μm in diameter, additional crossed polarized light images were collected at higher magnifications. The higher magnification images were collected using the 10×, 20×, 40×, and 50× objectives at camera resolutions of 1.36, 0.6, 0.34, and 0.27 μm/pixel, respectively. Multiple magnifications were used to provide overlap of the particle sizes to determine uncertainties in counting. One hundred images were collected at each magnification, which were distributed in a grid pattern within the area defined by the bounding rectangle of the print. Small differences in height across the area of the print required focusing of each image, which was accomplished by having the stage halt at the position of each image for manual focusing. Because some fields are empty, and thus completely dark, the automated focusing function encountered difficulties and was not used.

Particle Counting and Mass Determination from Microscopy

The RDX particles were sized and counted from the crossed polarized light images using an automatic bright particle thresholding procedure available in ImagePro. Any obvious fibers in the images were removed from the list of counted particles. The area of each particle was measured from the thresholded images, and the average diameter calculated on the basis of a circle of equivalent area. The data were binned by particle diameter into bins spaced at 1, 5, and 10 μm, and then every 10 μm to the largest particle present. The frequencies of the particle sizes from the higher magnification images were multiplied by the ratio of the total area of the bounding rectangle to the area sampled. No corrections were made for the fact that the print does not completely fill the bounding rectangle that defines the sampling space. For size bins smaller than 40 μm, the average and standard deviation were computed from the data obtained at multiple magnifications. No significant discontinuities were observed at the overlap of size bins from multiple magnifications. For size bins ≥40 μm, the tiled images supplied the data exclusively because of the ability to sample the entire area of the print. The frequencies of the larger particles are quite low, and sampling only a portion of the area, as is done for the higher magnification images, can introduce large uncertainties in counting.

The total mass of RDX was calculated from the particle size frequencies for six of the 50 prints. Masses were calculated using a density for RDX of 1.8 g/cm^3 (7) and a volume determined by the average diameter and either an average thickness, or a measured thickness. There were relatively few large particles in each print, and their thicknesses were directly measured. The smaller particles were too numerous, and therefore an average thickness based on measurements of over 270 particles from prints distributed over the

series was used. The thickness was measured from the difference in the *Z* position of the microscope stage between two focus positions, the base of the particle and the top of the particle. The accuracy in the *Z* position was tested by using the same procedure on calibrated glass spheres ranging in size from 7 μm in diameter to 74 μm in diameter. The calibration results showed a linear response ($r^2 = 0.999$) with a small positive error of *c.* 7% relative. Focusing on the top surface of the glass spheres is difficult, owing to a lack of features on the surface, and the small positive error was attributed to these difficulties. No corrections were made to the height measurements of the RDX particles.

Mass Determination from GC/μ-ECD

Six prints were selected following microscopic analysis to determine the amount of RDX by GC/μ-ECD. The entire fingerprint was extracted from each slide by visually identifying the location of the fingerprint, and then removing excess glass with a glass-cutter. The cut glass containing the fingerprint was placed in a short, wide-mouth jar (60 mL) and 5 mL of acetonitrile was added to completely cover the fingerprint. The fingerprint was sonicated for 10 min, and then five aliquots of solution, 500 μL each, were transferred to autosampler vials (1.7 mL).

Sample extracts were analyzed using a 6890N series GC/μ-ECD (Agilent, Palo Alto, CA). Separations were made in a Restek column with dimensions of 6 m × 0.5 mm (ID) × 1.5 μm film thickness. Pulsed split injections were made by autoinjector. Initial oven temperatures were 80°C, ramping to 180°C at 15°C/min, then to 190°C at 5°C/min, and finally to 220°C at 20°C/min. Injector and detector temperatures were 180°C and 300°C, respectively. An argon 95% + methane 5% make-up gas was maintained at a flow rate of 52 cc/min.

The system was calibrated using solutions of RDX in acetonitrile prepared from stock solutions (Accustandard, New Haven, CT) to cover the analytical range (0.05, 0.1, 0.25, 0.5, and 1.0 ng/μL of RDX). Prior to the calibration procedure, four solvent blanks (acetonitrile) were injected. During the analysis of the fingerprints, solvent blanks were injected at the beginning of the autosampling sequence and between each sample to prevent and monitor potential sample carryover. In addition, sample blanks were prepared by solvent extraction of a blank glass slide according to the procedure described above and analyzed prior to the fingerprint samples.

Results

The tiled, crossed polarized light images of 36 fingerprints from the series of 50 were processed to produce the image shown in Fig. 2. Each tiled image was thresholded, and then the contrast was inverted in order to show dark RDX particles against a light background. To enhance the visibility of the particles, a numeric label was used for each particle, which is assigned according to the position of the particle in the image. The numeric labels are larger than the particles, and therefore the images of the prints in Fig. 2 can be interpreted to show relative numbers and positions of RDX particles, but not their sizes. The particles are small enough that they would not be visible in the prints at the scale given in Fig. 2 without such enhancement.

There are some expected progressions in the series, including the change from the heavily loaded first few prints to the very lightly loaded last few prints. But it is also clear that there are significant heterogeneities in the series, both print to print and within a print. Within a print, the distribution of RDX particles can be very inhomogeneous, with the particles concentrating along the perimeter or along the front edge of the print. Particles are concentrated along

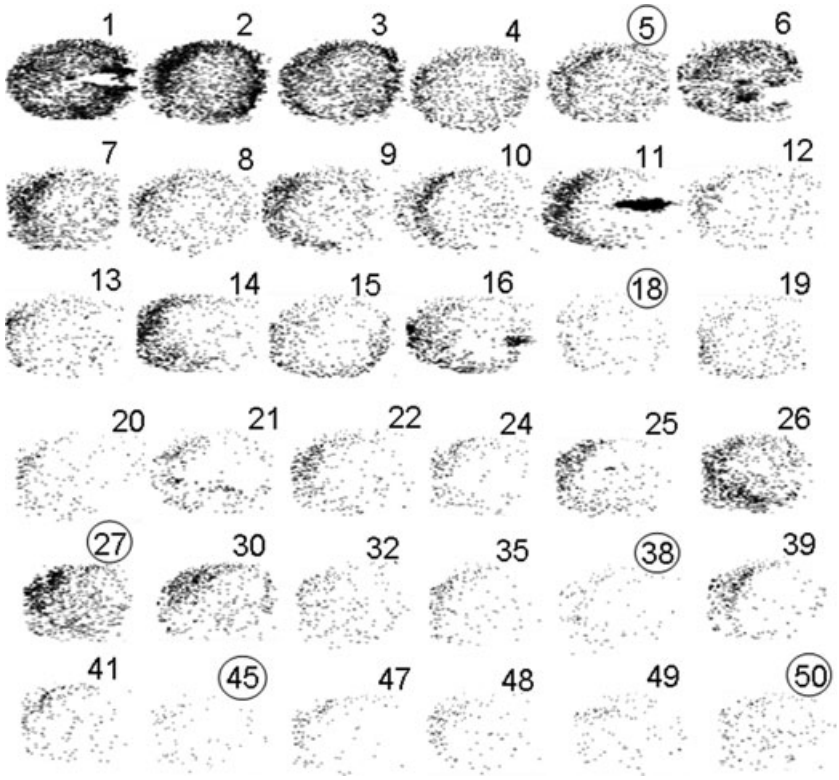

FIG. 2—*Thirty-six fingerprints from series of 50 showing positions of RDX particles. Fingerprints selected for analysis by GC/μ-ECD circled by number.*

the perimeter in prints 2 and 3, which indicates that material is pushed out to the edges in the initial stages of printing. There are unexpected features, such as the blank area within print 1 (which is also blank in the visible print image shown in Fig. 1). A heavy concentration of particles in print 11 mimics the shape of the blank area from print 1, suggesting that material may come off in discrete pieces. The prints do not exhibit a gradual progression from the heaviest loading to the lightest, but instead show significant variability. For example, prints 18 through 21 are in the middle of the series and have a relatively light loading, whereas prints 26, 27, and 30 show a much heavier loading. If the heterogeneity observed in this sequence is common for fingerprints prepared from C-4, it is easy to see how the prints prepared by Gresham et al. (3) would exhibit a high variability.

The particle size distributions for the prints agree with the results reported in our earlier study, with an increase in frequency with decreasing particle size consistent with a fragmentation process. Table 1 provides particle size distributions for selected prints. Thicknesses were measured for the largest particles for each of the prints listed in Table 1, and then for 10 randomly selected particles within each of the smaller size bins. The heights for only those particles that are single particles, and not agglomerates, were used to determine a thickness to width ratio that would describe the population of particles. There are agglomerates observed in the prints for which individual particles cannot be segregated in the thresholding process (Fig. 3). These are seen more frequently in the first few prints where the particle loading is relatively heavy. The thickness to width ratio for single particles has a mean value of 0.31, although the variability is quite large (Fig. 4). The thickness to width ratio is independent of the print number in the series, indicating that particles are not flattened by repeated pressure during print formation.

TABLE 1—*Particle size distributions from selected prints.*

d	P5		P18		P27		P38		P45		P50	
(μm)	*n**	mass (g)	*n*	mass (g)	*n*	mass (g)	*n*	mass (g)	*n*	mass (g)	*n*	mass (g)
1	20,374	3.7E-10	3221 (444)	5.8E-11	8273 (6645)	1.5E-10	2262	4.1E-11	1622 (1571)	2.9E-11	450 (269)	8.1E-12
5	7969 (7278)	1.8E-08	5941 (1062)	1.3E-08	7864 (4034)	1.8E-08	836 (617)	1.9E-09	893 (448)	2.0E-09	570 (124)	1.3E-09
10	670 (233)	1.2E-08	249 (115)	4.5E-09	680 (547)	1.2E-08	184 (78)	3.3E-09	178 (69)	3.2E-09	62 (41)	1.1E-09
20	221 (47)	1.1E-07	55 (2)	2.7E-08	196 (143)	9.5E-08	51 (8)	2.5E-08	38 (3)	1.9E-08	51 (30)	2.5E-08
30	43	8.9E-08	7	3.5E-08	46 (12)	1.1E-07	5	1.3E-08	8	1.5E-08	6	1.7E-08
40	5	2.0E-08	3	4.1E-08	11	4.5E-08	0	0	1	2.9E-09	5	5.1E-08
50	3	1.1E-07	0	0	1	4.7E-09	0	0	1	6.1E-09		9.6E-08
60	1	3.2E-09	0	0	3	2.0E-08	2	6.8E-08		4.8E-08		**2.3E-07**
70	2	7.2E-08	2	1.4E-07	0	0		1.1E-07		**1.9E-07**		
80	0	0	1	7.8E-08	1	2.6E-08		**1.3E-07**				
90	0	0		3.4E-07	1	8.0E-08						
100	1	1.7E-07		**2.7E-07**	0	0						
110	0	0			1	9.2E-08						
120	2	3.4E-07				5.0E-07						
130	0	0				**6.0E-07**						
140	0	0										
150	0	0										
160	1	1.0E-06										
		1.95E-06†										
		1.66E-06‡										

*Frequency (*n*) with uncertainty (1 SD) in parentheses is given for each size bin. The size bins are identified by the maximum diameter (*d*) of the particles in that bin.

†Masses calculated for each bin are summed at bottom of column.

‡Total RDX mass from each print determined by GC/μ-ECD analysis given in bold.

GC/μ-ECD, gas chromatography/μ-electron capture detection; RDX, hexahydro-1,3,5-trinitro-1,3,5-triazine.

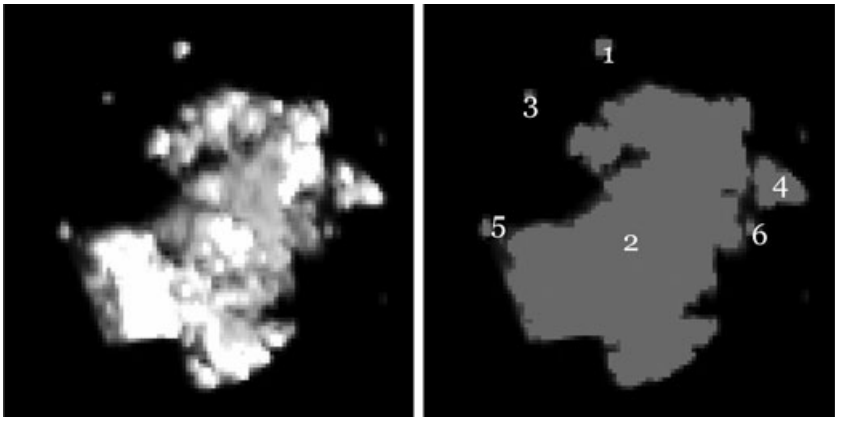

FIG. 3—*Agglomerated RDX particles from print 1 (left), where the center mass is counted as one particle in the thresholding process (right) with a diameter of 150 μm.*

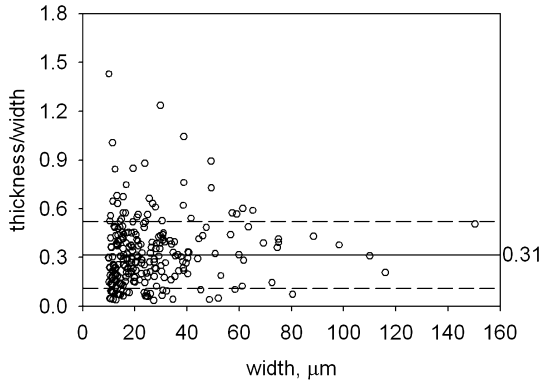

FIG. 4—*Thickness to width ratios for 270 single particles (not agglomerates) from prints identified in Table 1.*

Mass Determination

To calculate particle volumes, and thus mass, the measured particle thicknesses and diameters were used for particles in bin sizes of 30 μm or larger (40 μm or larger for print 27). The smaller particles were too numerous to measure particle thicknesses for each. For the smaller particles, volume was calculated using the average diameter of particles in the bin (e.g., 15 μm for 20 μm bin) and the average thickness to width ratio of 0.31. Volume was calculated based on two models for particle shape, a cylinder ($\pi r^2 h$) and a cone ($1/3\pi r^2 h$), where r is radius and h is height (thickness). The correspondence between the calculated mass from the particle measurements agreed most closely with the GC/μ-ECD measurements when a model intermediate to a cylinder and a cone was used, which is also the most physically reasonable shape. The masses calculated in Table 1 are based on this particle shape ($2/3\pi r^2 h$) and the corresponding mass determined by GC/μ-ECD for each print is given in bold. The largest uncertainties in the mass arise from uncertainties in the volume of the particles, overwhelming other sources of errors such as the counting errors listed in Table 1. The uncertainties in the mass measurements are therefore shown in Fig. 5*a* by indicating the range in values assuming the two end member shapes, the cylinder and the cone.

Despite the assumptions that must be used to calculate mass by particle counting, our estimates are quite good when compared with the GC/μ-ECD results. For the first four prints (5, 18, 27, and 38) the agreement between the two methods is within ±26% relative, and for the last two prints the biases in the particle-based estimates are −75% and −58% relative. This is quite good considering the mass of RDX varies from 1.7 to 130 ng. The mass estimates from particle counting are consistent with the progression through the series, showing the drop in mass for print 18 and then the increase for print 27. The total numbers of particles ≥10 μm in diameter, which can be counted in the tiled image, track this variability in mass from print to print (Fig. 5*b*). As a result, the images of the prints shown in Fig. 2 can be used to predict relative changes in mass through the series, although the size of the particles must be used to estimate the value. The ability to completely map the fingerprints and accurately count the large particles is critical to the success of this approach, as the mass is concentrated in the largest particles. Another case where attempts have been made to use particle counting to estimate mass is in asbestos analysis, and again the ability to count the largest particles is key (8).

There are a number of factors that can lead to bias in the estimation of mass by particle counting. Because we are using a fixed (nonrotating) stage, some percentage of the RDX particles will be

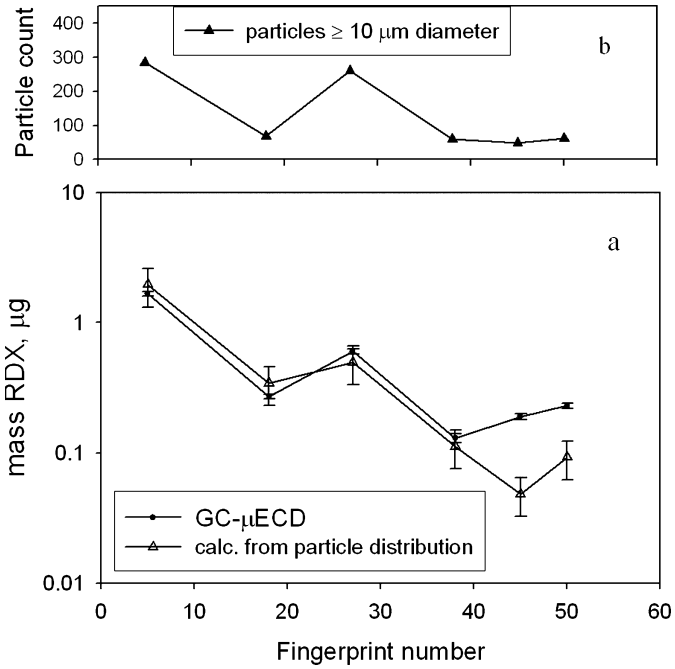

FIG. 5—*(a) Comparison of mass calculated from particle counts with GC/μ-ECD results for selected prints from series. The uncertainties for the GC/μ-ECD results are given as 1 SD. (b) Total particle counts for particles ≥10 μm in diameter shown for the same selected prints.*

dark under crossed polarized light because of their orientation. Assuming that a particle will be dark at ±2° of the extinction position, and that there are four extinction positions during a 360° rotation, every particle has a 4% chance of being dark at a given stage position. We did not observe any evidence of preferred orientation of the particles, and therefore we should have a loss of particles due to extinction of *c.* 4%. The relatively large negative bias for prints 45 and 50 may be due to the loss of a large particle(s) in the counting procedure. Particles can be missed because of extinction problems, or because they lay outside the boundaries of sampled area. The visibility of the last few prints was fairly low, and we may have missed a small portion of the active area of the print. There is also the possibility that some of the crystalline explosive in C-4 is actually octahydro-1,3,5,7-tetranitro-1,3,5,7-tetrazocine (HMX), which is often found mixed with RDX. HMX is more birefringent than RDX (9) and would be counted along with the RDX particles, but would not be detected by the GC/μ-ECD method as implemented. The presence of HMX would result in a positive bias by microscopy when compared with GC/μ-ECD.

The results of the mass distribution with respect to particle size can be used to evaluate strategies for improving detection. The strategy should take into account the probability of finding certain particle sizes in any sample (any fingerprint from the series), and the total mass that can be collected for that size bin. From the data given in Table 1, the average values of mass and particle frequency for the different size bins was calculated. These results are displayed graphically in Fig. 6. The diameter of each size bin was converted to that of an equivalent sphere. This was done to aid in evaluating particle sizes based on aerodynamic diameter, which is critical for understanding collection processes in personnel screening portals. The maximum particle size decreases throughout the fingerprint series, resulting in an average of less than 1 for particles greater than 40 μm in diameter. The smallest particles are present in every print, and therefore have much higher frequencies, but very small average masses. Even if all the particles in the smallest

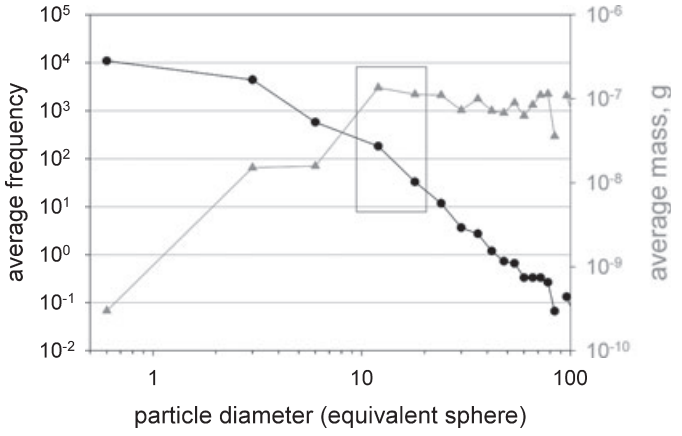

FIG. 6—*Frequency (circle) and mass (triangle) averaged for each size bin from Table 1. Particle diameter is converted to the diameter of a sphere of equivalent volume. The box encloses the particle diameters to target for sampling.*

size bin were collected, they would not be detected because the total mass (less than 1 ng) is below the detection limit of most IMS instruments. The most likely particle sizes to target for improved detection are those between 10 and 20 μm in diameter (inset box), as both frequency and mass are sufficient. To target particles smaller than 10 μm in diameter would require very efficient collection over a range of sizes, such that the sum of the particles would carry enough mass for detection.

Discussion

It is apparent from Fig. 2 that the process of transferring material to a surface via fingerprints is highly variable. It does not seem likely that any further control over the print making process could achieve reproducible prints. During preparation of the prints for this study, humidity, temperature, and applied force were controlled, the printing surfaces were all prepared in the same manner, and the C-4 sample was prepared in a way to ensure a controlled loading on the thumb. However, during the print making process, a change in the feel of the material was observed from print to print that was thought to be due to changes in material pliability. A change in the workability of the material may be unavoidable and may result in an uneven release of material.

Because prints cannot be made in a reproducible manner, they must be analyzed individually to determine the mass of RDX. Because of the extreme variability, it is not sufficient to measure the prints preceding and following the target print and interpolate a value. For example, analyzing prints 10 and 12 would not provide accurate information on print 11. For this reason, the type of procedure proposed by Gresham et al. (3) for generating standards for ETD testing would be subject to a high uncertainty. The variability in print production necessitates a method such as the one proposed in this paper, which can characterize the print, provide an estimate of the mass, and does so in a nondestructive manner. Our method does have limitations, in that the background must be isotropic. We have measured prints from glass slides and silicon wafers (in reflected light), and similar isotropic substrates would also work. Another limitation is the uncertainty in the mass determination as previously discussed. A potential use of the prints is for studies of sampling efficiency, such as those described in Phares et al. (5). In this case, a relative measure of the sampled mass can be determined by counting the particles remaining in the print after sampling. Since the mass is concentrated in particles ≥10 μm in diameter, tiling the print after sampling will be sufficient to determine sampling efficiency.

Although we collected high magnification images to sample the particles smaller than 10 μm, this is not necessary to evaluate the mass of RDX. The particles smaller than 10 μm have high frequencies, but represent a small proportion (11% or less) of the total mass. An error of 11% or less is well within the error budget of the technique. The tiled images can be used exclusively to characterize a fingerprint, which means that the analysis of each print can be completed in a relatively short time. The heights of the largest particles should be measured for accuracy, especially for particles with diameters exceeding 100 μm. Use of the average height to width ratio is sufficient for particles smaller than *c.* 50 μm in diameter.

The method described in this paper works well for C-4 fingerprints because RDX has a high birefringence, and because the background components are generally isotropic. Plastic explosives containing pentaerythritol tetranitrate (PETN) are more challenging because of the low birefringence of PETN. We are currently working on an approach for imaging PETN in Detasheet and Semtex H, two explosive formulations that are typically included in a list of potential threats.

References

1. Eiceman GA, Stone JA. Ion mobility spectrometers in national defense. Anal Chem 2004;1:390A–7A.
2. Hallowell SF. Screening people for illicit substances: a survey of current portal technology. Talanta 2001;54:447–58.
3. Gresham GL, Davies JP, Goodrich LD, Blackwood LG, Liu BYH, Thimsem D, et al. Development of particle standards for testing detection systems: mass of RDX and particle size distribution of composition 4 residues. In: Lawrence AH, editor. Proceedings Volume 2275 of the SPIE Conference, Cargo Inspection Technologies, 1994;34–44.
4. Reardon MR, Bender EC. Differentiation of composition C-4 based on the analysis of the process oil. J Forensic Sci 2005;50(3):1–7.
5. Phares DJ, Holt JK, Smedley GT, Flagan RC. Method for characterization of adhesion properties of trace explosives in fingerprints and fingerprint simulations. J Forensic Sci 2000;45(4):774–84.
6. Verkouteren JR. Particle characteristics of trace high explosives: RDX and PETN. J Forensic Sci 2007;52(2):335–40.
7. Armstrong RW, Elban WL. Materials science and technology aspects of energetic (explosive) materials. Mater Sci Technol 2006;22(4):381–95.
8. Wylie AG. Modeling asbestos populations: a fractal approach. Can Mineral 1993;30:437–46.
9. McCrone WC, Andreen JH, Tsang SM. Identification of organic high explosives. Microscope 1993;41:161–82.

Additional information and reprint requests:
Jessica L. Coleman, M.S.
National Institute of Standards and Technology
100 Bureau Drive, Stop 8371
Gaithersburg, MD 20899
E-mail: jessica.coleman@nist.gov